REPORT

OPTICS

Photonic doping of epsilon-near-zero media

Iñigo Liberal,[1]* Ahmed M. Mahmoud,[1,2]* Yue Li,[1,3]* Brian Edwards,[1] Nader Engheta[1]†

Doping a semiconductor with foreign atoms enables the control of its electrical and optical properties. We transplant the concept of doping to macroscopic photonics, demonstrating that two-dimensional dielectric particles immersed in a two-dimensional epsilon-near-zero medium act as dopants that modify the medium's effective permeability while keeping its effective permittivity near zero, independently of their positions within the host. The response of a large body can be tuned with a single impurity, including cases such as engineering perfect magnetic conductor and epsilon-and-mu-near-zero media with nonmagnetic constituents. This effect is experimentally demonstrated at microwave frequencies via the observation of geometry-independent tunneling. This methodology might provide a new pathway for engineering electromagnetic metamaterials and reconfigurable optical systems.

Doping—the judicious inclusion of impurities into a material, with the aim of controlling the material's macroscopic parameters—has been essential in the development of the semiconductor industry (*1*). Arguably, the success of semiconductor devices lies largely in the possibility of engineering their electrical, optical, and/or magnetic properties with a relatively small number of randomly located impurities. For instance, tailoring the electrical conductivity via doping facilitated the development of diodes and transistors, which are the basis of microelectronics (*2*). Different doping mechanisms are also central to a number of optical and optoelectronic devices, including lasers, light-emitting diodes, and solar cells (*3*).

In principle, the concepts behind doping could be transplanted to other structures, length scales, and, in general, fields of physics. This was successfully done, for instance, when applying doping principles from bulky semiconductors to nanocrystals or quantum dots (*4*). In our work, the concept of doping is applied to the fields of macroscopic photonics and electromagnetic metamaterials (*5*, *6*) and, in particular, media with near-zero parameters (*5*, *7*–*9*). However, the extrapolation is nontrivial. In fact, when a homogeneous host body, characterized by macroscopic material parameters such as relative permittivity ε_h and relative permeability μ_h, is filled with a macroscopic dopant (characterized by ε_d and μ_d), this foreign body scatters the internal electromagnetic fields, and the response of the system in general differs from that of a homogeneous body with effective macroscopic parameters ε_{eff} and μ_{eff}.

Traditionally, it is only in the long-wavelength regime that a body filled with impurities can be substituted with a homogenized body by using suitable effective-medium theories (EMTs) (*10*). Conventional EMTs apply usually under three conditions: The original body must contain a sufficiently large number of impurities, and both their size and separation must be much smaller than the wavelength of operation (*10*). Although these conditions are actually relaxed in advanced homogenization techniques (*11*, *12*), these processes break down and inevitably lose their physical meaning as the size of the impurities increases and their numbers decrease (*13*). In general, a homogeneous body containing a few disordered impurities cannot be modeled and homogenized by using effective parameters, limiting the generalization of the doping paradigm to macroscopic photonic systems.

However, within epsilon-near-zero (ENZ) media, the wavelength is effectively stretched (*5*, *7*–*9*), leading to large phase velocities and static-like field distributions. This could potentially relax the requirements for a physically sound homogenization process, and we demonstrate that impurities immersed locally in ENZ media behave as doping agents that tune the media's global effective permeability. This technique may provide a pathway to engineer the electromagnetic response of structures with near-zero parameters, as well as their associated photonic phenomena, which include tunneling (*8*, *9*, *14*, *15*), geometry-invariant resonant cavities (*16*), highly directive (*7*, *17*) and collective (*18*) emission, enhanced nonlinear response (*19*–*21*), and bound states in the continuum (*22*–*24*).

As depicted in Fig. 1A and fig. S1 (*25*), we first consider a two-dimensional (2D) ENZ body of arbitrary cross-sectional shape and area A, containing one or more disordered 2D impurities characterized by area A_d, relative permittivity ε_d, and permeability μ_d. By solving the pertinent boundary value problem [see supplementary note 1 (*25*)], we found that all fields excited external to the ENZ body in a generic 2D scattering scenario with the magnetic field polarized along the z axis (i.e., perpendicular to the 2D plane) are identical to those of a homogeneous ENZ body with effective relative permeability and permittivity given by

$$\mu_{eff} = 1 + \sum_d \Delta\mu_d,\ \varepsilon_{eff} = 0 \qquad (1)$$

where the variation of the effective relative permeability induced by the dth impurity is given by

$$\Delta\mu_d = \frac{1}{A}\left[\int_{A_d} \psi^d(\mathbf{r})dA - A_d\right] \qquad (2)$$

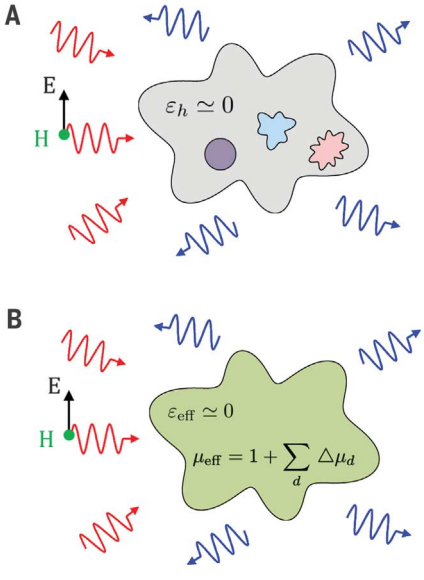

Fig. 1. Conceptual sketch of photonic doping. (**A**) A 2D epsilon-near-zero (ENZ) body (relative permittivity $\varepsilon_h \approx 0$, relative permeability $\mu_h = 1$) with an arbitrary cross-sectional shape, doped with several 2D macroscopic nonmagnetic dielectric impurities and illuminated with an electromagnetic wave whose magnetic field H is polarized along the out-of-the-plane axis. (Note that this incident wave is not necessarily a plane wave; i.e., it can be waves and fields from a nearby source.) (**B**) The equivalent homogeneous 2D body (as seen by an outside observer) with the same cross-sectional shape and near-zero permittivity ($\varepsilon_h \approx 0$), but with a uniform effective permeability, following Eqs. 1 and 2, noting its additive contributions to effective permeability from the nonmagnetic impurities. None of the constituent material in (A) is magnetic (i.e., its relative permeability is unity), yet the effective permeability of the structure in (B) can be different from unity. E, electric field; H, magnetic field.

[1]Department of Electrical and Systems Engineering, University of Pennsylvania, Philadelphia, PA 19104, USA. [2]Department of Physics, The American University in Cairo, Cairo, Egypt. [3]Department of Electronic Engineering, Tsinghua University, Beijing 100084, China.
*These authors contributed equally to this work.
†Corresponding author. Email: engheta@ee.upenn.edu

Here, $\psi^d(\mathbf{r})$ is the magnetic field distribution within the impurity, normalized such that $\psi^d(\mathbf{r}) = 1$ on its boundary [see supplementary note 1 (*25*)]. $\Delta\mu_d$ is solely determined by the properties of the 2D dopant (i.e., its cross-sectional geometry and constitutive parameters) and the overall area of the host. In other words, $\Delta\mu_d$ is independent of the external geometry of the ENZ host's cross-sectional shape, as well as the position of and the interaction between the impurities within it. Macroscopic 2D particles immersed in a 2D ENZ body therefore play a role analogous to that of electronic dopants, in the sense that they affect the macroscopic photonic response of the whole body in an additive manner.

The effective permittivity of the host is unchanged by the presence of dopants—that is, $\varepsilon_{eff} = 0$ [see supplementary note 1 (*25*)]. We emphasize that μ_{eff}, as defined in Eq. 1, is not an approximation obtained, for example, via field averaging. On the contrary, in the ENZ limit, μ_{eff} (and the fact that ε_{eff} of the entire body remains zero) provides an exact representation of the external fields, including both near and far fields. The effective permeability and effective permittivity shown in Eq. 1 are able to predict the response of entire doped bodies with arbitrary cross sections, as well as their interaction with arbitrary incident fields (e.g., even those excited by sources placed in the vicinity of the doped body). This result also holds even if the ENZ body is immersed in a complex environment with several external dielectric bodies [see fig. S1 (*25*)].

For an ENZ host, the concept of doping can thus be extrapolated to the fields of macroscopic photonics and electromagnetic metamaterials. We believe that this result provides an alternative pathway to the design of artificial electromagnetic materials. For instance, on the basis of Eqs. 1 and 2, one can readily infer the effect of different classes of impurities in the response of the ENZ body. For example, small 2D dielectric particles, whose radius r_d is much smaller than the free-space wavelength λ_0 ($r_d \ll \lambda_0$), with positive $\varepsilon_d > 0$ (or negative $\varepsilon_d < 0$) permittivity induce a paramagnetic $\Delta\mu_d > 0$ (or diamagnetic $\Delta\mu_d < 0$) behavior given by $\Delta\mu_d \approx \varepsilon_d(\pi A_d^2)/(2A\lambda_0^2)$. Good conducting particles (i.e., those larger than the penetration depth) induce a diamagnetic response proportional to their area $\Delta\mu_d = -A_d/A$. Additional cases are detailed in supplementary note 2 (*25*).

The proposed theoretical framework remains valid even if the sizes of the dopants are comparable to or even larger than the wavelength of operation, opening the possibility of exploring resonant doping effects. In turn, this enables the control of a large scatterer with a single, arbitrarily located impurity of potential application for reconfigurable photonic devices. As a case study, we consider a circular nonmagnetic ($\mu_d = 1$) dielectric rod of radius r_d and relative permittivity ε_d. Its contribution to the effective permeability is given by $\Delta\mu_d = (A_d/A)\{[2/(k_d r_d)][J_1(k_d r_d)/J_0(k_d r_d)] - 1\}$, where $J_n(\cdot)$ represents the cylindrical Bessel function of the first kind and order n, and $k_d = \omega\sqrt{\varepsilon_d}/c$ (where ω is the radian frequency and c is the vacuum speed of light).

This dopant presents a clear resonant behavior at $J_0(k_d r_d) = 0$. To illustrate this point, Fig. 2 depicts the effective permeability of an arbitrarily shaped 2D ENZ body of cross-sectional area $A = 2\lambda_0^2$, containing a single 2D dielectric rod impurity ($\mu_d = 1$, $\varepsilon_d = 10$), as a function of the rod radius r_d. At resonance, we get $\mu_{eff} \to \infty$, and the fields excited outside the body are identical to those excited by a perfect magnetic conductor (PMC) body. This implies, for example, that the fields excited by a 2D emitter located in the vicinity of the doped body are primarily reflected by it (Fig. 2C), such that the emission is directed into a single half-space (Fig. 2C, right). Furthermore, in contrast to good (electric) conducting materials, the electric field on the surface of the PMC body is not zero but maximized. Therefore, the reflection from the body does not inhibit but, on the contrary, enhances the local electric field at the position of the emitter, thus accelerating the radiation process. In general, PMC bodies are of great interest as they exhibit opaque high-impedance surfaces (*26*), empowering efficient emission, perfect absorption, and directional scattering with a planar profile.

Above resonance, the effective permeability becomes negative and eventually crosses zero. At this point, the fields excited outside the body are identical to those of an epsilon-and-mu-near-zero (EMNZ) body ($\mu_{eff} \approx 0$, $\varepsilon_{eff} \approx 0$). EMNZ bodies provide interesting wave physics associated with a zero-index behavior while being impedance-matched to free space for normal incidence (*7*). As shown in Fig. 2D, this results in enhanced transmission through the body (Fig. 2D, center), as well as in the formation of highly directive beams perpendicular to the sides of the body (Fig. 2D, right). These features

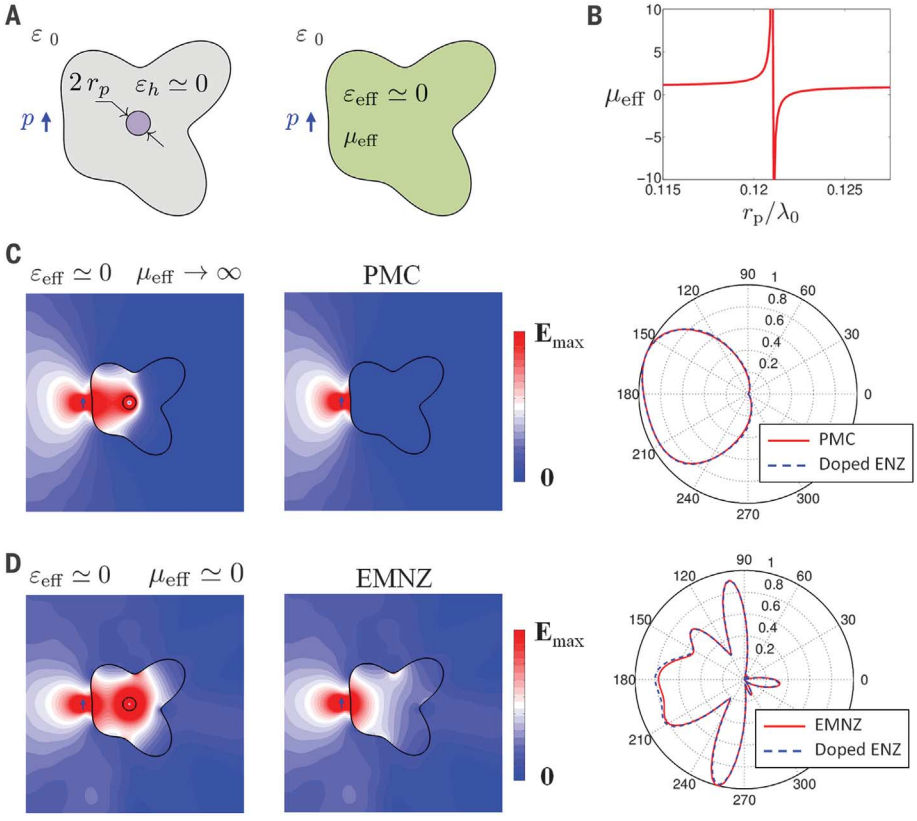

Fig. 2. Photonic doping with a single impurity. (**A**) (Left) Sketch of the geometry of our scattering objects: a 2D ENZ body of arbitrary cross-sectional shape and area $A = 2\lambda_0^2$ (λ_0, free-space wavelength), photonically doped with a single 2D impurity consisting of a dielectric rod of relative permittivity $\varepsilon_d = 10$ and radius r_p. A 2D electric-line dipole source, with dipole moment p, is placed outside in the vicinity of the body. (Right) As seen by an outside observer, the 2D body appears as a body with the same shape, with effective parameters shown in the figure. (**B**) Effective relative permeability of the ENZ body as a function of the rod radius. (**C** and **D**) Numerical predictions of the electric field magnitude distributions (left and center panels) and the normalized power radiation pattern (right panel) for (C) $\mu_{eff} \to \infty$ [i.e., perfect magnetic conductor (PMC)] and (D) $\mu_{eff} \approx 0$ [i.e., epsilon-and-mu-near-zero (EMNZ)] cases. These figures represent a comparison between the implementation via doped ENZ (left panel) and their equivalent bodies (center panel), such as PMC and EMNZ structures with the same cross-sectional shapes. The external fields are the same for each case and its equivalent body (but not the internal fields). The results illustrate the possibility of controlling the scattering properties of a large body with a single impurity.

of EMNZ media have been exploited in the past to achieve directive emission (*7*, *17*), geometry-invariant tunneling (*27*), and anomalous scattering properties (*28*).

The numerical simulations reported in Fig. 2 illustrate an excellent agreement between the responses of PMC and EMNZ media and their implementations via photonic doping. Small deviations are due to numerical accuracy only, as the result is exact for ideal material parameters [see supplementary note 1 (*25*)]. A parametric analysis of the effect of losses on the excited fields is reported in fig. S2. Moderate losses [Im(ε) < 0.03] do not have a dramatic influence, primarily resulting in dampened scattered fields while a similar spatial distribution is maintained. The results are also independent of the position of the rod, as shown in figs. S3 and S4 (*25*), for the lossless and lossy cases, respectively. The external fields are independent of the positions of the impurities; hence, an external observer (who only analyzes the fields at the ENZ frequency) will not obtain any information on the internal positions of the particles. Although the external fields are identical, the internal fields do necessarily change as a function of the position of the particle [see fig. S3 (*25*)]. A more in-depth analysis of photonic doping in the presence of an absorbing and dispersive host can be found in supplementary note 3 and supplementary figs. S5 and S6 (*25*).

Therefore, we conclude that by doping a 2D ENZ body with a single arbitrarily located impurity, it is possible to effectively tune its permeability, including extreme cases such as PMC and EMNZ responses. Furthermore, the response of the body could also be dynamically tuned between these or other cases by changing the rod's permittivity and/or radius. In this manner, the properties of the entire body, potentially spanning several wavelengths, would be controlled with a single small actuator with an arbitrary location. More importantly, although conventional metamaterials (typically based on periodic structures) have difficulty maintaining the validity of the effective parameters on complex geometries (e.g., when the local curvature of a boundary becomes comparable to the size of the unit cells composing the metamaterial), our methodology provides a pathway to the design of PMC and EMNZ bodies with intricate or even deformable surfaces.

We provide an experimental proof-of-concept demonstration of photonic doping by implementing EMNZ tunneling (*27*) at microwave frequencies. The advantages of this approach are twofold: First, the experimental demonstration is carried out in a closed and controlled environment. Second, EMNZ behavior is characterized by a clear signature (i.e., resonant transmission with zero phase advance), independently of the geometrical shape of the waveguide deformation (*27*), which is distinct to EMNZ media.

Photographs of the experimental setup are shown in Fig. 3A. Additional details can be found in supplementary notes 4 to 6, as well as in figs. S7 to S9 (*25*). Our design consists of an EMNZ test region inserted between two metallic rectangular waveguides, acting as input and output ports and supporting the fundamental TE_{10} mode. The entire structure (test region and waveguide ports) is configured as two parallel metallic plates with a separation in the z axis of $h = \lambda_0/2$ at the frequency of operation $\omega_0 = 2\pi \times 2.376 \times 10^9$ rad/s. This causes the empty test region to be at the cutoff frequency for the TE_{10} mode, which is known to exhibit ENZ properties (*15*). The input and output waveguides are filled with dielectric materials ($\varepsilon_{diel} = 2$) so that they can function above the TE_{10} cutoff. These waveguides have a width of $\lambda_0/3$ such that they are monomodal across the frequency range of the experiment.

To demonstrate the geometry-invariant properties of EMNZ tunneling, as well as the position independence and geometry invariance of photonic doping, we tested three different cavity geometries and three separate dielectric rod locations within each geometry, giving a total of nine different experiments. All structures have the same cross-sectional area of $1.37\lambda_0 \times 1.37\lambda_0$: The first cavity (Fig. 3A, top) is characterized by a simple rectangular geometry, and the ports are located to conform a 90° bend. The second cavity (Fig. 3A, middle) has an arbitrary cross-sectional shape, designed by using a random-number generator, and splines while maintaining the same cross-sectional area and the same orthogonal port orientation. The third cavity (Fig. 3A, bottom) was designed similarly, but the ports are located rather arbitrarily and are not oriented orthogonal to each other. As it will be subsequently demonstrated, high resonant transmission is observed at the design frequency in all nine configurations despite the large and evident changes in geometry.

The ENZ region is "doped" with a single circular dielectric rod of radius $r_d = 0.137\lambda_0$, and

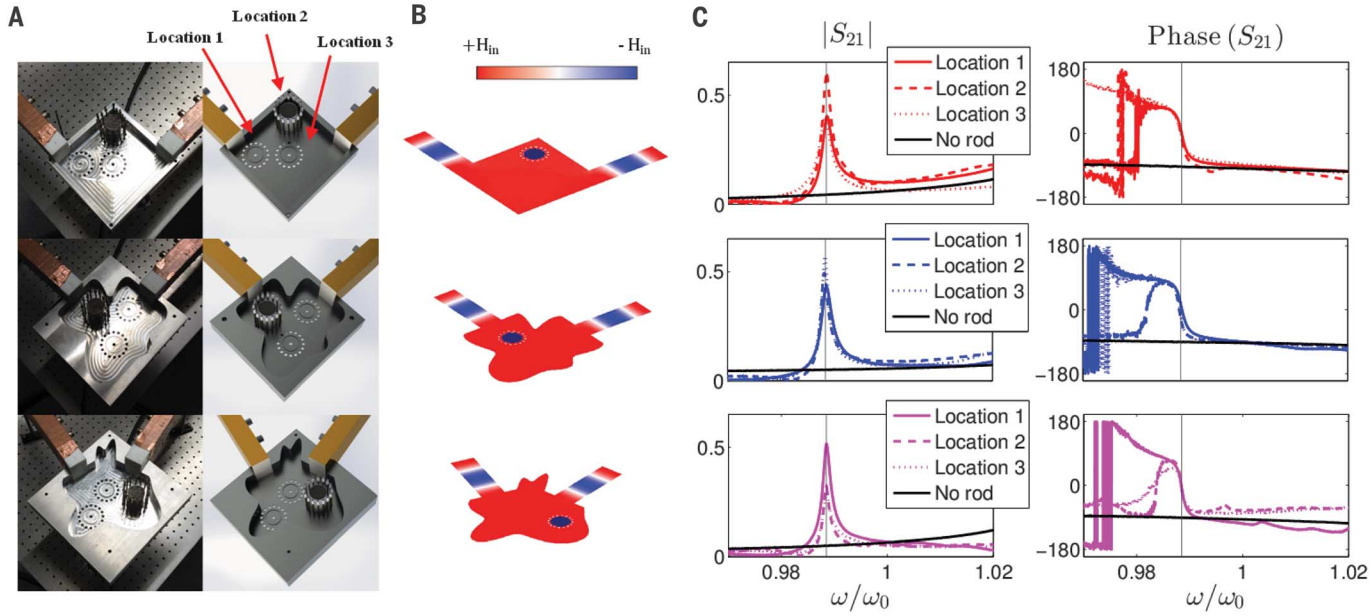

Fig. 3. Experimental demonstration of EMNZ tunneling facilitated via photonic doping. (**A**) Photograph and sketch of the experimental setup: three different EMNZ regions (waveguide-at-cutoff–based ENZ structure with a dielectric rod as the dopant) connected with input and output waveguides. Each cavity contains three possible locations for a dopant consisting of a circular dielectric rod. (**B**) Snapshot of the numerically predicted magnetic field in the middle plane in each cavity ($z = h/2$, where h is the waveguide height), illustrating full transmission with zero phase advance. (**C**) Measurement of the magnitude, $|S_{21}|$, and phase, Phase(S_{21}), of the transmission coefficient of the three cavities (red, blue, and magenta) and in each cavity for the three different locations (solid, dashed, and dotted lines) of the dielectric dopant. A peak of transmission with zero-phase crossing is consistently observed in all configurations and pinned to the same EMNZ frequency, demonstrating geometry-invariant EMNZ tunneling, as well as position-independent and geometry-invariant photonic doping. ω, radian frequency of the input signal.

relative permittivity $\varepsilon_d = 9$, designed to induce an EMNZ behavior at the frequency of operation. To avoid the excitation of additional modes (*29*), we surrounded the perimeter of the dielectric rod with 16 conductive (3.18-mm copper) wires, as shown in Fig. 3A. Details of the operation and assembly of the wires can be found in supplementary note 5 and figs. S8 and S9 (*25*).

First, we numerically analyzed the experimental setup with a commercial full-wave numerical solver (*30*). Figure 3B represents snapshots of the numerically predicted magnetic field in the middle plane ($z = h/2$) within the structure when it is illuminated by a wave coming from one of the ports. Regardless of the shape of the EMNZ section and the location of the dielectric rod, the EMNZ behavior is preserved with resonant transmission and almost no phase progression through the structure. The predicted magnetic field is uniform in phase and amplitude across the structure in all cases, despite the relatively large area and the substantial differences between the structures. A comprehensive numerical analysis of the experimental setup is reported in figs. S10 to S13 and described in supplementary note 7 (*25*).

The measured transmission coefficients are gathered in Fig. 3C, and a peak in the transmission coefficient magnitude is consistently observed in all nine measurements. Although the frequency positioning of the transmission peak is shifted 1% from the prescribed value, it does not shift with changes on the rod's location or section geometry, thus evidencing the position-independent and geometry-invariant properties of photonic doping. Furthermore, the peak in the transmission coefficient is consistently accompanied by a zero-crossing in phase for all nine cases. This is an unequivocal signature of geometry-invariant EMNZ tunneling, in which a large physical volume that would have otherwise influenced the electromagnetic wave propagation externally behaves as a "single point" electromagnetically, as viewed from the external world (*27*). The frequency shift observed in the transmission coefficient is ascribed to small inaccuracies in the rod permittivity value and/or the imperfect fabrication of the wire mesh. Figure 3C also includes the measured transmission coefficients in the absence of the dielectric rod (black solid line), for which the transmission peak disappears. This ratifies that the tunneling effect does not occur because of ENZ tunneling [which only takes place for small waveguide cross sections (*8*)] or any other resonant effect related to the shape of the cavities. From a practical standpoint, this result demonstrates that the effective permeability and scattering properties of a large, arbitrarily shaped ENZ body can be controlled with a single impurity, independently of its location.

Despite the practical interest in controlling the macroscopic response of a large body with a single or very few dopants, noteworthy physical phenomena also arise in the superdense doping case—that is, when many small dopants force the filling factor to asymptotically approach one (i.e., $f = \sum_d A_d/A \to 1$). In common macroscopic mixtures, the effective parameters asymptotically approach those of the dominant phase when its filling factor approaches one (*10*). However, the same principle does not apply in ideal ENZ media. For instance, if an ENZ body is filled with many electrically small dielectric rods ($k_d r_d \ll 1$), each one providing a small paramagnetic contribution $\Delta\mu_d = \varepsilon_d(\pi A_d^2)/(2A\lambda_0^2)$, as the filling factor f approaches one, the effective permeability exhibits only a small paramagnetic effect: $\mu_{eff} \to 1 + \varepsilon_d A_d/(2\lambda_0^2)$, with $A_d/\lambda_0^2 \ll 1$. As shown in Fig. 4, this implies that it is possible to densely dope an ENZ host without affecting its macroscopic response to electromagnetic fields. In the most extreme conceptual case, one could envision filling the ENZ body with a fractal distribution such that the area of the host asymptotically approaches zero (but the ENZ region is still connected) while having no effect on its electromagnetic response at the ENZ frequency. From a more practical perspective, this finding suggests the possibility of engineering the mechanical and/or thermal properties of a device (e.g., by using a porous material) without affecting its electromagnetic response at the ENZ frequency.

Many other phenomena might emerge in the superdense doping regime. For instance, if the ENZ host is heavily doped with perfect electric conductor (PEC) particles, the effective permeability asymptotically approaches zero as the filling factor increases: $\mu_{eff} = 1 - \sum_d A_d/A \to 0$. That is to say, an ENZ body densely doped with PEC impurities asymptotically approaches the response of an EMNZ medium. As illustrated in Fig. 4C via numerical simulations, this counterintuitively implies that a larger presence of PEC bodies within the ENZ host results in better matching to the host's external region and smaller reflection and scattering. From this perspective, early investigations on ENZ tunneling in narrow channels (*8*, *14*) can be reinterpreted as a particular implementation of PEC doping. In fact, if we periodically arranged the structure shown in Fig. 4C, thus forming a PEC-doped slab, a normally incident plane wave would be tunneled through it with negligible reflection [see fig. S14 (*25*)]. In general, from a theoretical perspective, one finds that under certain circumstances a 2D body whose cross-sectional area is mostly occupied by PEC particles (but still surrounded by ideal ENZ, albeit a very thin layer of ENZ) could be transparent to electromagnetic fields. From a more practical standpoint, this result could be applied to enhance nonlinearity in ENZ media [as demonstrated by recent experiments involving ENZ nonlinear optics (*19*–*21*)]. In particular, this result indicates that an ENZ body could be doped with good conductor particles (e.g., silver) to facilitate the penetration and concentration of the electric field in the ENZ sample, thus boosting nonlinear processes.

Our theoretical and experimental results demonstrate that the effective permeability of a 2D ENZ body can be tuned with the addition of macroscopic impurities whose contributions are additive and independent of any interaction between the impurities and/or their locations within the host. Because the size, number, and location of the impurities, as well as the shape of the host, are arbitrary, this result is fundamentally different from previous effective medium and metamaterial theories. The proposed concept is derived for 2D systems and, in principle, cannot be

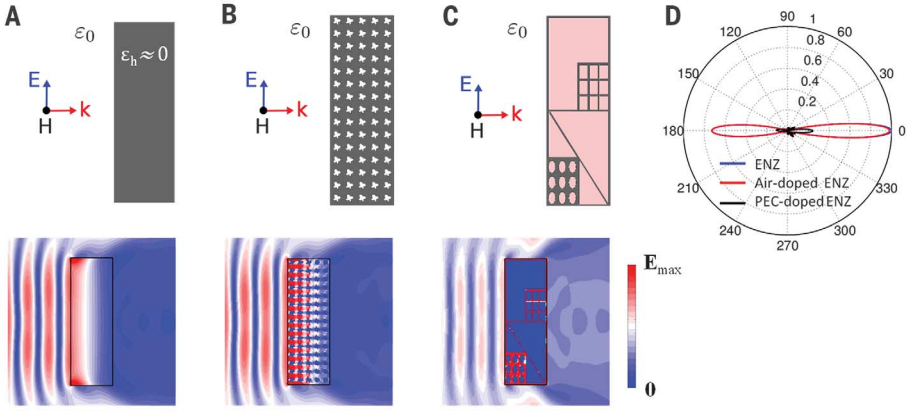

Fig. 4. Superdense photonic doping. (**A**) Sketch of the geometries and numerically predicted electric field magnitude distribution for a λ_0-by-3λ_0 2D ENZ slab illuminated by a plane wave with the magnetic field polarized along the *z* axis. k, propagation constant of the incident wave. (**B** and **C**) Same as in (A), but the ENZ slab has been densely doped with (B) 75 arbitrarily shaped identical air impurities ($\varepsilon_d = 1$) of area $A_d = \pi(0.05\lambda_0)^2$ or (C) perfect electric conductor (PEC) 2D regions of different shapes and sizes [shown in pink in the top panel of (C)] embraced by the ENZ region [shown in gray in the top panel of (C)]. (**D**) Comparison between the scattering-power patterns of the original, air-doped, and PEC-doped ENZ slabs. The results confirm two counterintuitive effects: (i) Polluting a 2D ENZ body with deeply subwavelength 2D dielectric particles (even many particles) has a negligible effect on its response to an external source, and (ii) heavy doping with arbitrarily shaped PEC regions reduces scattering and reflection.

directly translated to arbitrary 3D systems. However, these concepts can be implemented and measured in 3D physical systems in which the variation of the fields is fixed or predetermined in one direction. This is the case, for example, in our experimental verification in a single-mode waveguide system. A similar behavior can be obtained with 3D bodies with a high-aspect ratio, where the field along one axis asymptotically becomes uniform [see fig. S15 (*25*)]. We believe that it provides a new pathway to engineer electromagnetic metamaterials and structures with near-zero parameters, as well as their associated photonic phenomena. Specific examples of the potential scientific and technological applications of this concept might include reconfigurable and flexible photonics (with a single small actuator that is arbitrarily located), nonlinear optics (with enhanced field penetration in the ENZ host), and quantum metamaterials.

REFERENCES AND NOTES

1. S. M. Sze, K. N. Kwok, *Physics of Semiconductor Devices* (Wiley, ed. 3, 2006).
2. A. S. Sedra, K. C. Smith, *Microelectronic Circuits* (Oxford Univ. Press, 1998).
3. P. Würfel, U. Würfel, *Physics of Solar Cells: From Basic Principles to Advance Concepts* (Wiley-VCH, ed. 3, 2016).
4. S. C. Erwin *et al.*, *Nature* **436**, 91–94 (2005).
5. N. Engheta, R. W. Ziolkowski, *Metamaterials: Physics and Engineering Explorations* (IEEE-Wiley, 2006).
6. G. V. Eleftheriades, K. G. Balmain, *Negative-Refraction Metamaterials: Fundamental Principles and Applications* (Wiley, 2005).
7. R. W. Ziolkowski, *Phys. Rev. E* **70**, 046608 (2004).
8. M. Silveirinha, N. Engheta, *Phys. Rev. Lett.* **97**, 157403 (2006).
9. M. G. Silveirinha, N. Engheta, *Phys. Rev. B* **75**, 075119 (2007).
10. A. H. Sihvola, *Electromagnetic Mixing Formulas and Applications* (IET, 1999).
11. Y. Wu, J. Li, Z. Q. Zhang, C. T. Chan, *Phys. Rev. B* **74**, 085111 (2006).
12. A. Alù, *Phys. Rev. B* **84**, 075153 (2011).
13. P. M. T. Ikonen, E. Saenz, R. Gonzalo, C. R. Simovski, S. A. Tretyakov, *Metamaterials* **1**, 89–105 (2007).
14. M. G. Silveirinha, N. Engheta, *Phys. Rev. B* **76**, 245109 (2007).
15. B. Edwards, A. Alù, M. E. Young, M. Silveirinha, N. Engheta, *Phys. Rev. Lett.* **100**, 033903 (2008).
16. I. Liberal, A. M. Mahmoud, N. Engheta, *Nat. Commun.* **7**, 10989 (2016).
17. S. Enoch, G. Tayeb, P. Sabouroux, N. Guérin, P. Vincent, *Phys. Rev. Lett.* **89**, 213902 (2002).
18. R. Sokhoyan, H. A. Atwater, *Opt. Express* **21**, 32279–32290 (2013).
19. M. Z. Alam, I. De Leon, R. W. Boyd, *Science* **352**, 795–797 (2016).
20. L. Caspani *et al.*, *Phys. Rev. Lett.* **116**, 233901 (2016).
21. A. Capretti, Y. Wang, N. Engheta, L. Dal Negro, *Opt. Lett.* **40**, 1500–1503 (2015).
22. M. G. Silveirinha, *Phys. Rev. A* **89**, 023813 (2014).
23. F. Monticone, A. Alù, *Phys. Rev. Lett.* **112**, 213903 (2014).
24. I. Liberal, N. Engheta, *Sci. Adv.* **2**, e1600987 (2016).
25. See supplementary materials.
26. D. Sievenpiper, Z. Lijun, R. F. J. Broas, N. G. Alexopoulos, E. Yablonovitch, *IEEE Trans. Microw. Theory Tech.* **47**, 2059–2074 (1999).
27. A. M. Mahmoud, N. Engheta, *Nat. Commun.* **5**, 5638 (2014).
28. V. C. Nguyen, L. Chen, K. Halterman, *Phys. Rev. Lett.* **105**, 233908 (2010).
29. C. Della Giovampaola, N. Engheta, *Phys. Rev. B* **93**, 195152 (2016).
30. The numerical calculations were all performed in COMSOL Multiphysics 5.0 (available at www.comsol.com).

ACKNOWLEDGMENTS

We acknowledge partial support from the Vannevar Bush Faculty Fellowship program, sponsored by the Basic Research Office of the Assistant Secretary of Defense for Research and Engineering and funded by the Office of Naval Research through grant N00014-16-1-2029, and partial support from the U.S. Air Force Office of Scientific Research Multidisciplinary University Research Initiative Awards FA9550-12-1-0488 and FA9550-14-1-0389. Y.L. acknowledges partial support from the National Natural Science Foundation of China under grant 61301001. All data used to obtain our conclusions are present in the main paper and/or the supplementary materials. Additional data related to this paper may be requested from N.E.

SUPPLEMENTARY MATERIALS

www.sciencemag.org/content/355/6329/1058/suppl/DC1
Supplementary Text
Figs. S1 to S15
References (*31*–*33*)

23 October 2016; accepted 13 February 2017
10.1126/science.aal2672

Editor's Summary

Doped photonics

Doping semiconductor materials with impurity atoms enables control of the optoelectronic properties that enhance functionality. Liberal *et al.* describe numerically and experimentally an analogous doping effect for a group of photonic materials. They introduced a dielectric into an otherwise nonmagnetic material, which produced a magnetic response. The generality of the method should allow the design of photonic materials with enhanced and controlled electromagnetic response.

Science, this issue p. 1058